

Integration of Concentrating Solar Power With High Temperature Electrolysis for Hydrogen Production

Zhiwen Ma^{1,*}  and Janna Martinek¹ 

¹National Renewable Energy Laboratory (NREL), Golden, Colorado 80401, USA

*Correspondence: Zhiwen.ma@nrel.gov

Abstract. Hydrogen has been identified as a leading sustainable contender to replace fossil fuels for transportation or electricity generation, and hydrogen generated from renewable sources can be an energy carrier for a carbon-free economy. Several hydrogen production methods are under development or deployment with various technical readiness levels and techno-economic potentials. This study focuses on integrating concentrating solar thermal power (CSP) with high temperature electrolysis (HTE) using solid oxide electrolysis cells (SOEC). The CSP-HTE integration approach provides the benefits of thermal energy storage for continuous operation, improved capacity, and reduced thermal cycling for improved SOEC life. The CSP-HTE system analysis utilizes a Python-based system modeling program in connection with solar receiver thermal output derived from the NREL System Advisor Model (SAM) software. The system model facilitates component sizing, performance simulation, and evaluation of operation modes on an annual basis for various CSP-HTE configurations including CSP with thermal energy storage (TES). The SOEC operation conditions were simulated to assess component sizing and performance and to derive system capacity factors.

Keywords: Concentrating Solar Thermal Power, High Temperature Electrolysis, Solid Oxide Electrolysis Cell, Renewable Hydrogen

1. Introduction

Hydrogen (H₂) is attractive in mitigating greenhouse gas emissions and global warming. Low costs, high energy density, and existing infrastructure make fossil fuels convenient sources of energy supply and, as a result, these fuels are difficult to replace with renewable sources. Thus, H₂ produced from renewable energy sources must be affordable and able to support broad industry applications with various production paths in order to displace fossil fuels.

The difficulty and energy intensity of water splitting has resulted in broad research areas in search of effective methods for hydrogen production from water [1]. Fig. 1 shows a range of approaches under development from photoelectrochemical and photocatalytic water splitting to water electrolysis and thermochemical water splitting. Four methods of H₂ production are under development including photoelectrochemical cell (PEC), proton exchange membrane electrolysis cell (PEMEC), solid oxide electrolysis cell (SOEC), and solar thermochemical hydrogen (STCH) [2]. Each method can be divided into subcategories as shown in Fig. 1.

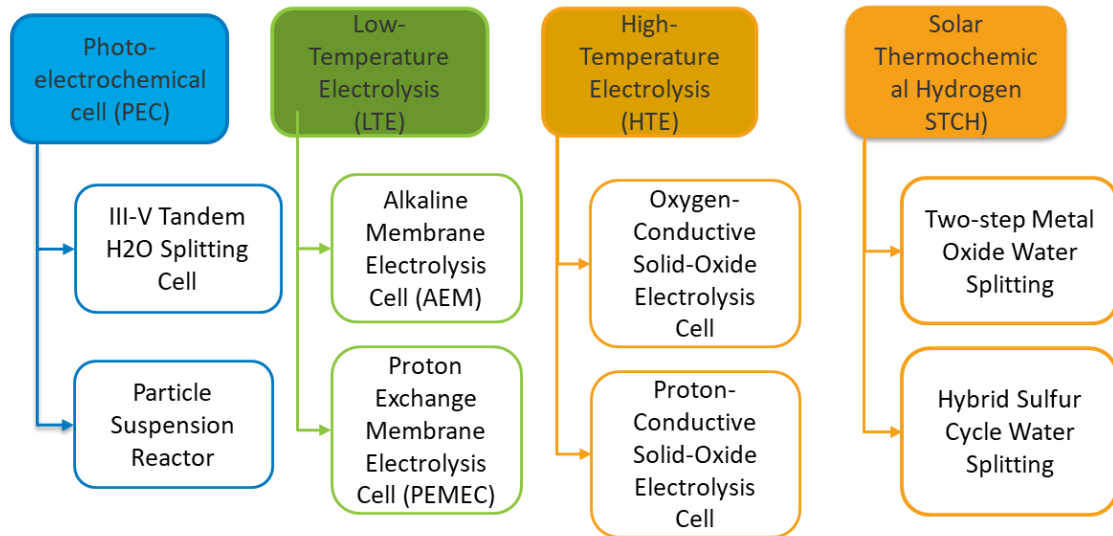


Fig. 1: Various H₂ production paths explored in the U.S. DOE HydroGEN program [2].

Photoelectrochemical and photocatalytic water splitting converts solar energy to hydrogen by using sunlight directly at ambient temperature. These processes utilize photoelectrolytic cells with an integrated internal photovoltaic component to drive an electrolysis process to split water into hydrogen and oxygen [3]–[5]. Tandem semiconductor cells combine photovoltaic electric supply with electrolysis water splitting [3], [5], while particle suspension reactors incorporate photocatalysts suspended in water to assist a direct reaction [4]. Both methods are in the research stage and have gaps towards practical uses. The electrochemical water splitting is divided into low temperature electrolysis (LTE) using polymer membrane electrolyte, or high temperature electrolysis (HTE) using solid oxide electrolyte. A LTE process consumes electricity at a rate 50-55 kWh/kgH₂ at efficiencies of 60-70%, which is the major cost barrier to achieve a \$2/kgH₂ production target in addition to the capital cost of the LTE components. HTE methods working at ~600°C (proton-conductive solid oxide electrolysis cell, or P-SOEC) and ~800°C (oxygen conductive electrolysis cell, or O-SOEC) reduce electric power consumption by electrolyzing steam at a lower electrical voltage, while low-cost heat from solar or nuclear sources can supplement the energy use, resulting in about 20% reduction of electric consumption.

Thermochemical and solar thermochemical hydrogen production could refer to a broad range of high-temperature processes, including those relying on initial carbonaceous feedstocks. In Fig. 1 we focus on specifically on solar thermochemical water splitting redox cycles. These process use twostep or multi-step metal oxide redox cycles and can avoid electricity usage by directly reducing metal oxide at high temperatures (~1,500°C) and splitting water at a lower temperature (~1,000°C) [6]. The reaction temperatures depend on the characteristics of the metal oxide, and currently ceria and novel perovskite materials are the most studied materials. Reaction temperatures exceeding 1,000°C for two-step STCH processes still pose challenges for concentrating solar thermal power (CSP) components such as the solar receiver and TES. STCH technology requests a new approach in CSP solar receiver design and feasible TES method. Thus, STCH development so far is still focused on material research and uncertainties in CSP integration.

CSP can provide heat and/or electricity to HTE H₂ production processes although nuclear power has been considered as a main source to supply heat and electricity to the electrolysis process. CSP technologies use mirrors to focus solar energy and project it onto a solar receiver. Depending on the mirror and receiver layouts, CSP technologies can be categorized as line focus solar collectors such as parabolic troughs or linear Fresnel, and point focus solar collectors such as power tower and parabolic dishes. Each CSP type offers various solar con-

centration conditions and optimum operating temperatures that can support STCH or integration with HTE processes for water splitting [7]–[10]. Parabolic trough and power tower configurations are the most widely used CSP technologies that provide suitable temperature ranges to integrate with HTE of water. In addition, O-SOEC has been developed to a more mature stage compared to P-SOEC. This paper focuses on CSP integration with O-SOEC to assess system performance.

2. CSP-HTE System Integration

Fig. 2 shows a high-level block diagram of CSP integration with the HTE O-SOEC subsystem. In the basic model the CSP system supplies heat to the O-SOEC steam and sweep gases, with heat recuperation from the O-SOEC products. The electric source can be CSP driven power generation with TES [11] (not shown in Fig. 2), or it can also be sourced from photovoltaic or grid power with a renewable source [1], [12].

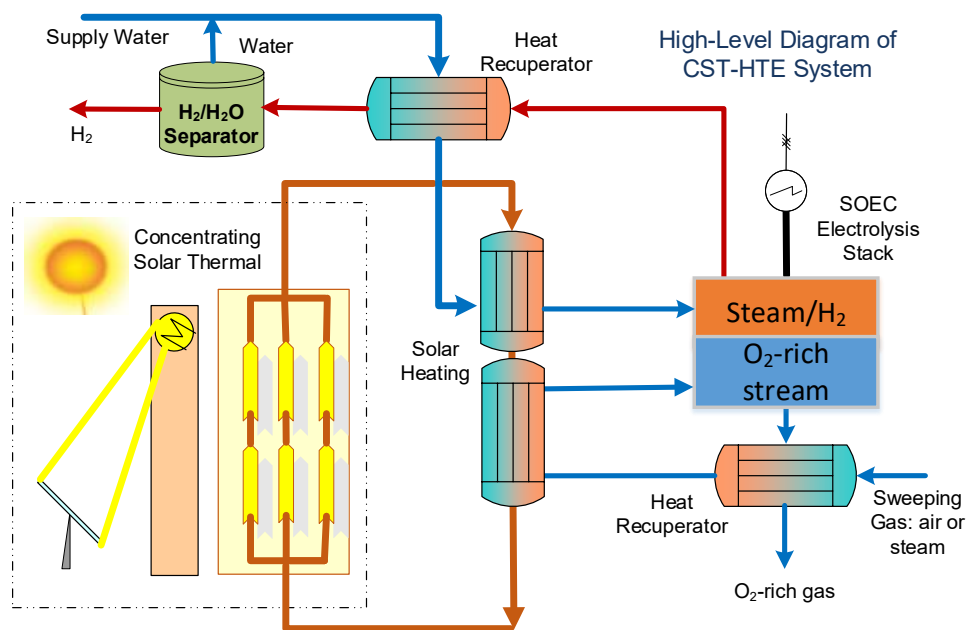


Fig. 2: A schematic of CST-HTE integration to support O-SOEC H₂ production.

A CSP-HTE integrated system provides benefits of supplying high-temperature heat from the CSP to the SOEC electrolysis process. Both CSP configurations of parabolic trough and power tower can supply heat and electricity; however, power tower CSP can provide higher temperature heat and more effective TES than a parabolic trough system. TES associated with power tower CSP can provide continuous supply of heat and power for SOEC operation or to maintain the SOEC in a hot standby state. Correspondingly, TES can minimize SOEC thermal cycling and benefit cell life while also increasing the plant capacity factor. CSP with molten-salt TES has been demonstrated commercially at 100 MWe with 10 hrs of storage capacity, is a suitable system to integrate with SOEC for HTE of water and is the focus of this analysis.

3. CSP-HTE System Modeling

3.1. System Diagram of HTE-CSP-TES integration

Fig. 3 illustrates a flow diagram of the simulated CSP and high temperature electrolysis (CSP-HTE) process, including key components of the CSP system, O-SOEC subsystem, heat recuperation, trim heaters, and balance of plant components. The flow diagram is based on a process diagram for an O-SOEC system (FuelCell Energy [13]). The TES is charged from CSP

and provides heat and/or electricity with consideration of various operation options. We simulate commercial molten salt power tower technology using a nitrate salt heat transfer fluid (HTF) and storage media with a hot storage temperature of 565°C. The CSP-TES system drives a steam Rankine cycle for power generation.

As illustrated in Fig. 3, the thermal demands of the process for steam evaporation and superheating are supplied by the CSP system, with a small additional contribution from trim heaters that raise the temperature of O-SOEC inlet streams to the O-SOEC operating temperature and make up for imperfect heat recuperation. Electrical demands are dominated by the O-SOEC, but also include requirements for the compressors, pumps, cooling tower, and trim heaters, as well as parasitic loads associated with operation of the solar field, receiver, and power cycle. These electrical demands are supplied by either the CSP power cycle alone, or in combination with an on-site PV array in the model. Additionally small portions of the CSP plant parasitic loads are allowed to be derived from grid electricity in the model at some points in time. For simplicity, the power cycle driven by the molten-salt TES is not simulated directly and instead described by a design point thermal-to-electric efficiency and relative part load performance.

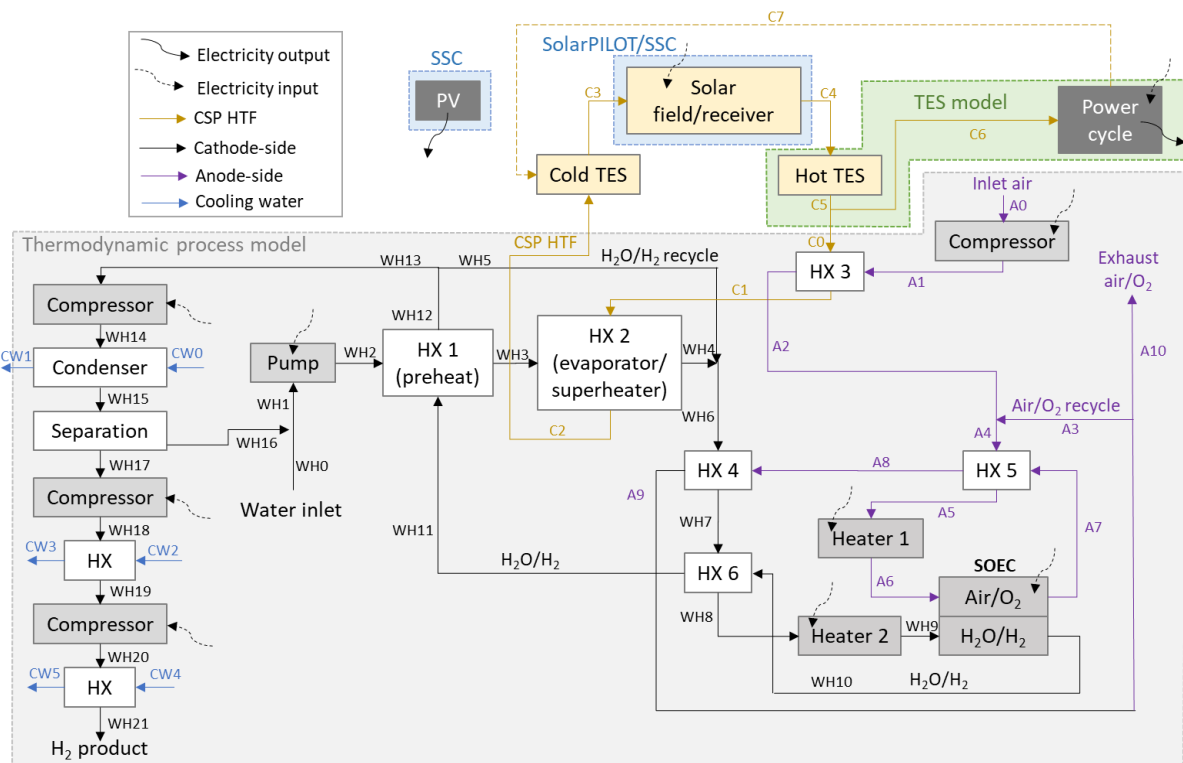


Fig. 3: System flow diagram: Highlighted regions delineate components of the performance models including (1) Thermodynamic process and SOEC (design point conditions only), (2) Solar components, and (3) TES dispatch and annual performance.

Table 1 lists base case input values for the mass and enthalpy balance solutions describing design point operation of the HTE process (grey shaded region in **Fig. 3**). The hourly H₂ production rate in **Table 1** provides 50,000 kg/day H₂ if the process is operated at design point conditions for 24 hours per day. The CSP nominal hot storage temperature is well under the SOEC operating temperature; however, with the extensive heat recuperation illustrated in **Fig. 3**, the heat demand supplied by the electric heaters accounted for only approximately 0.75 kWh/kg H₂, less than 8% of the heat delivered from CSP to the HTE process in **Fig. 3** (9.8 kWh/kg H₂) at the base case parameters in **Table 1**.

Table 1. Base case plant specification and process model parameters

Parameter	Value	Parameter	Value
H ₂ production rate	2083.3 kg/hr	Compressor or pump isentropic efficiency	0.8
SOEC operating T	800°C	Compressor or pump mechanical efficiency	0.9
SOEC operating P	5 bar	Trim heater electric-to-thermal efficiency	1.0
SOEC voltage	Thermoneutral	CSP HTF	60% NaNO ₃ / 40% KNO ₃
Cathode inlet H ₂ O mole fraction	0.9	CSP hot storage T	565°C
H ₂ O utilization fraction	0.8	CSP cold storage T	290°C
Anode inlet O ₂ mole fraction	0.25	Cooling water supply T	20°C
Anode outlet O ₂ mole fraction	0.4	Cooling water return T	35°C
Sweep gas or water inlet T	25°C	Condenser pressure	5 bar
Sweep gas or water inlet P	1 bar	Intermediate H ₂ pressure	10 bar
Heat exchanger effectiveness	0.9	Final H ₂ pressure	20 bar

3.2. Thermodynamic process model and SOEC model

The HTE process (grey-shaded region in Fig. 3) is assumed to operate only at steady state and at design point conditions described in **Table 1**. Thermal and electrical demands of the process are calculated by solving mass, species, and energy balances for all components. Key assumptions in the calculations include (1) steady state operation, (2) fixed effectiveness of all heat exchangers (within limitations imposed by constraints disallowing phase change in HX1 in Fig. 3), (3) negligible pressure drop across the SOEC, heat exchangers, and trim heaters, (4) ideal gas behavior in all compressors, (5) fixed isentropic efficiency and mechanical efficiency for all compressors and pumps, (6) negligible cooling tower electrical demand, (7) isothermal SOEC operation with no heat losses to the environment, and (8) channel-average SOEC species compositions. Iterative solutions for the heat and mass balances are required due to the recycle streams and heat recuperation network. Models were solved in Python using a sequence of nested iterations to converge all mass and energy balances and to determine the water/air inlet flow rates, recycle fractions, and CSP HTF flow rate to achieve the target SOEC inlet/outlet conditions and target CSP cold storage return temperature.

The SOEC is simulated with a lumped parameter model in the porous media, neglecting variation in species composition within the axial flow direction in the gas channels and instead assuming channel-average species compositions. The charge transfer reaction is assumed to occur only at the electrode-electrolyte interface. The cell is assumed to operate at the thermoneutral voltage, and the operating voltage and current density are calculated accounting for activation, concentration and ohmic overpotentials derived in [14] and applied for SOEC modeling in [15] as these were found to provide a better fit to V-I data than the standard form of the Butler Volmer equations.

3.3. Modeling of solar integration, TES, and CST-HTE system performance

Two configurations are considered: one with CSP alone, and a second incorporating a PV array to supply all or part of the electricity demands during the day, with the CSP system supplementing electrical supply when the PV output is below the total process electrical requirement and supplying the thermal requirements anytime the HTE process is operating or in standby. Full 24/7 operation of the HTE process cannot be achieved without an extremely high solar multiple and TES capacity that is unlikely to be economically optimal, and thus annual performance analysis is necessary to approximate an annual capacity factor, and to discern the relationship between solar component sizing, annual capacity factor, and H₂ cost.

Sizing of the CSP solar components is based on a solar multiple (defined here as the ratio of the receiver capacity at design point conditions, relative to the sum of the design point HTE process thermal requirement and the thermal-equivalent of the HTE process electrical requirement assuming a fixed CSP power cycle efficiency). Heliostat layouts, tower height and receiver sizing for the corresponding receiver thermal capacity are optimized using SolarPILOT. The power cycle is sized based on the HTE electrical demands and an assumed net-to-gross power ratio. Hourly thermal outflow from the CSP receiver and hourly field/receiver parasitic loads are calculated using the NREL SAM simulation core (SSC) [16]. Time-series energy balances and dispatch of the TES system are solved outside of the SAM environment and consider available hourly inflow from the field/receiver ($q_t^{rec,av}$), discharge of stored energy to operate the HTE process and provide CSP plant parasitic loads (q_t^{disch}), defocusing of energy from the field receiver to avoid exceeding TES capacity ($q_t^{defocus}$), and a small hourly loss rate (f^{loss}). The discharge rate from storage depends on the HTE process operational mode, CSP parasitic loads, and PV generation (in cases where PV is included). CSP power cycle parasitic loads are approximated by a fixed parasitic load (relative to cycle capacity) and a variable parasitic load (fixed fraction of cycle gross generation) that are approximated based on default input parameters in the SAM molten salt power tower (MSPT) model.

$$Q_t^{TES} = Q_{t-1}^{TES}(1 - f^{loss}) + (q_t^{rec,av} - q_t^{defocus} - q_t^{disch})\Delta t \quad (1)$$

When PV is included, the PV inverter is sized based on a PV multiple (defined here as the design point AC output relative to the HTE process electrical requirement) and the PV array is sized with a fixed DC-to-AC power ratio. Excess PV can be used for CSP parasitic loads and HTE process standby electrical requirements, and any excess not utilized locally is assumed to be curtailed or sold to the grid. The scenarios of sales of excess PV electricity or storing it in TES for off-sun power generation can add value to the system by reducing energy cost.

Table 2 provides base case input parameters for the CSP and PV integration. All parameters pertaining to the SSC calculations that are not specified here are set to SAM default parameters. Note that solar multiple(s) and thermal storage capacities represent preliminary values, and have not yet been optimized relative to cost of H₂.

Table 2. Base case input parameters for CSP and PV simulations

Parameter	Value
CSP technology and HTF	Molten salt power tower, 60% NaNO ₃ / 40% KNO ₃
TES hot storage T / cold storage T	565°C / 290°C
Solar resource	Daggett, CA, TMY2
Design point DNI	950 W/m ²
Solar multiple	2.5
TES capacity	14 hours (CSP only), 18 hours (CSP + PV)
TES hourly loss	0.042% per hour (~1% per day)
Design point cycle efficiency	0.412
Part-load cycle performance (fit to Rankine cycle [17])	$\frac{\eta}{\eta^{des}} = 0.6992 + 0.5691\left(\frac{q}{q^{des}}\right) - 0.2697\left(\frac{q}{q^{des}}\right)^2$
Assumed cycle net-to-gross power ratio	0.95
Cycle pump and condenser parasitic loads	0.0265 x Cycle gross generation
CSP fixed parasitic load	0.0055 x Cycle gross capacity
HTE process standby thermal demand	25% of thermal demand during operation
PV multiple	1.5

4. Results and Discussions

The model requires that the thermal and electrical demands of the HTE process shown in Table 3 be met by the CSP or CSP+PV system at every hour, and determines when to put

the HTE process in a hot standby mode that consumes only a small quantity of thermal energy from the TES. The HTE annual operation model is intended to produce an initial estimate of capacity factor and does not account for numerous operational details including CSP cycle startup requirements, ramping constraints, ambient-temperature variation of cycle efficiency, temperature variability or off-design conditions in the HTE process, variation of power cycle return temperature and cold storage temperature etc. In addition to CSP and PV system sizing and capital costs, the key result that connects performance simulation to techno-economic analysis is annual capacity factor. For a base CSP-only case solar multiple of 2.5 (with 14 hours of TES) our calculations predict a capacity factor of approximately 63% based on Daggett, CA TMY weather, increasing to 84% when a PV array sized to provide 1.5 times the SOEC electrical demand under nominal conditions (and additional 4 hours of TES) are added to the system.

Table 3 provides base case annual performance metrics using input parameters in Tables 1 and 2. The annual solar-to-H₂ efficiency shown in The HTE annual operation model is intended to produce an initial estimate of capacity factor and does not account for numerous operational details including CSP cycle startup requirements, ramping constraints, ambient-temperature variation of cycle efficiency, temperature variability or off-design conditions in the HTE process, variation of power cycle return temperature and cold storage temperature etc. In addition to CSP and PV system sizing and capital costs, the key result that connects performance simulation to techno-economic analysis is annual capacity factor. For a base CSP-only case solar multiple of 2.5 (with 14 hours of TES) our calculations predict a capacity factor of approximately 63% based on Daggett, CA TMY weather, increasing to 84% when a PV array sized to provide 1.5 times the SOEC electrical demand under nominal conditions (and additional 4 hours of TES) are added to the system.

Table 3 is defined in equation (2), and does not include the minor parasitic or standby electrical requirements that are allowed to be supplied from the grid.

$$\eta_{solar-to-H_2}^{an} = \frac{\int_0^{8760} \dot{n}_{H_2} HHV_{H_2} dt}{\int_0^{8760} [(DNI)A_{helio} + (DNI + DHI)A_{pv}] dt} \quad (2)$$

The HTE annual operation model is intended to produce an initial estimate of capacity factor and does not account for numerous operational details including CSP cycle startup requirements, ramping constraints, ambient-temperature variation of cycle efficiency, temperature variability or off-design conditions in the HTE process, variation of power cycle return temperature and cold storage temperature etc. In addition to CSP and PV system sizing and capital costs, the key result that connects performance simulation to techno-economic analysis is annual capacity factor. For a base CSP-only case solar multiple of 2.5 (with 14 hours of TES) our calculations predict a capacity factor of approximately 63% based on Daggett, CA TMY weather, increasing to 84% when a PV array sized to provide 1.5 times the SOEC electrical demand under nominal conditions (and additional 4 hours of TES) are added to the system.

Table 3. Base case annual performance results

Output	CSP only (14 hours TES)	CSP + PV (18 hours TES)
Receiver design point thermal capacity (MWt)	522 MWt	522 MWt
Receiver height, diameter (m)	16.7 m, 16.0 m	16.7 m, 16.0 m
Tower height (m)	172 m	172 m
Number of heliostats (12.2 x 12.2 m)	6833	6833
Cycle design point gross electrical capacity (MWe)	81.7	81.7
Annual CSP electricity used for the HTE process (GWhe)	427.9	321.6
Annual PV electricity used for the HTE process (GWhe)	0.0	249.6
Annual CSP electricity used for CSP parasitic loads (GWhe)	18.9	11.5

Annual PV electricity used for CSP parasitic loads (GWhe)	0.0	8.6
CSP parasitic loads from the grid (GWhe)	6.6	0.7
Excess PV generation (or curtailment) (GWhe)	0.0	44.9
Standby electrical demands assuming operation of BOP components (GWhe)	7.6	2.5
Annual HTE process capacity factor	0.629	0.840
Annual solar-to-H₂ efficiency	0.164	0.117

Fig. 4 illustrates a heat map of annual hourly operational modes for the HTE process for the CSP-only and CSP-PV scenarios. In the CSP-PV case the system operates using PV electricity during the day (supplemented with part-load CSP power cycle operation during early morning, late afternoon, or wintertime periods), and operates using electricity from the CSP power cycle at night. This increases the annual capacity factor but also substantially increases power cycle ramping and startup/shutdown cycling as the power cycle was allowed to operate around the variable PV without constraint.

Exact values for the thermal and electrical requirements for the standby mode were unknown and can alter the capacity factor as TES dispatched to supply standby requirements reduces the total available for HTE operation. However, results indicated that the uncertainty in standby requirements is only a minor concern, with the annual capacity factor for the CSP-only case varying between 63.8% to 60% when considering the bounding cases with either no TES dispatch required or with the full HTE process thermal requirements required for standby.

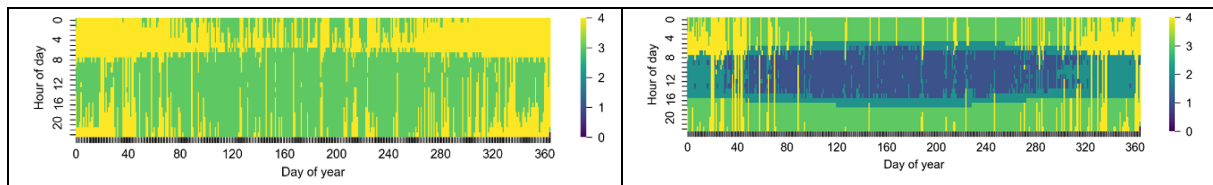


Fig. 4: Annual heat map of HTE process operational states for CSP-only and CSP+PV cases. Process states — 0: Off, 1: On with PV electricity, 2: On with PV+CSP electricity, 3: On with CSP electricity, 4: Standby.

5. Conclusions

Hybridizing CSP with HTE technology such as solid oxide electrolysis cells is promising for producing H₂ from solar energy at a temperature compatible with CSP operation. A CSP-HTE or CSP-PV-HTE system model has been developed including component integration and approximate annual performance analysis to evaluate the integration of CSP with HTE. Incorporating CSP with thermal energy storage supports HTE hot standby conditions to avoid HTE thermal cycling. The results shown here demonstrate a methodology for calculating the hourly performance, system capacity factor, and annual hydrogen production for a given combination of CSP, TES, and PV capacities; however, the results for annual solar-to-H₂ efficiency are not an indication of the favorability of the CSP-only vs. the CSP-PV hybrid system as only system performance is considered and not the relative capital or operating costs of the technologies. The annual system performance model can provide a basis for future techno-economic analysis and system design optimization for comparison of CSP-HTE and CSP-PV-HTE on the basis of levelized cost of hydrogen. Additional future analysis may consider optimized operational strategies to balance annual productivity and thermal cycling of the CSP components in the hybrid CSP-PV-HTE configuration. Hybridizing PV and CSP can be a path to achieve low electric cost, while high-efficiency power generation and low-cost TES are future development paths to reduce the cost of H₂ production.

Competing interests

The authors declare no competing interests.

Data availability statement

Data is available upon request to the authors.

Author contributions

Zhiwen Ma: Conceptualization, Supervision, Funding Acquisition, Writing – Outline and Draft Revision. **Janna Martinek:** Conceptualization, Methodology, Analysis, Writing –Draft, Results Visualization.

Acknowledgement

This work was authored by the National Renewable Energy Laboratory, operated by Alliance for Sustainable Energy, LLC, for the U.S. Department of Energy (DOE) under Contract No. DE-AC36-08GO28308. Funding provided by the U.S. Department of Energy Office of Energy Efficiency and Renewable Energy Solar Energy Technologies Office and Hydrogen and Fuel Cell Technologies Office. The views expressed in the article do not necessarily represent the views of the DOE or the U.S. Government. The U.S. Government retains and the publisher, by accepting the article for publication, acknowledges that the U.S. Government retains a non-exclusive, paid-up, irrevocable, worldwide license to publish or reproduce the published form of this work, or allow others to do so, for U.S. Government purposes.

References

- [1] A. Mohammadi and M. Mehrpooya, "A comprehensive review on coupling different types of electrolyzer to renewable energy sources," *Energy*, vol. 158, pp. 632–655, 2018, doi: 10.1016/j.energy.2018.06.073.
- [2] H. N. Dinh, A. Weber, A. Mcdaniel, and R. Boardman, "HydroGEN : A Consortium on Advanced Water Splitting Materials, DOE Hydrogen and Fuel Cells Program, FY 2019 Annual Progress Report," 2019.
- [3] M. Grätzel, "PECreview," *Nature*, vol. 414, no. November, pp. 338–344, 2001.
- [4] D. M. Fabian et al., "Particle suspension reactors and materials for solar-driven water splitting," *Energy Environ. Sci.*, vol. 8, no. 10, pp. 2825–2850, 2015, doi: 10.1039/c5ee01434d.
- [5] J. L. Young, M. A. Steiner, H. Döscher, R. M. France, J. A. Turner, and T. G. Deutsch, "Direct solar-to-hydrogen conversion via inverted metamorphic multi-junction semiconductor architectures," *Nat. Energy*, vol. 2, no. 4, pp. 1–8, 2017, doi: 10.1038/nenergy.2017.28.
- [6] Z. Ma, P. Davenport, and G. Saur, "System and technoeconomic analysis of solar thermochemical hydrogen production," *Renew. Energy*, vol. 190, pp. 294–308, 2022, doi: 10.1016/j.renene.2022.03.108.
- [7] N. Monnerie, H. von Storch, A. Houaijia, M. Roeb, and C. Sattler, "Hydrogen production by coupling pressurized high temperature electrolyser with solar tower technology," *Int. J. Hydrogen Energy*, vol. 42, no. 19, pp. 13498–13509, 2017, doi: 10.1016/j.ijhydene.2016.11.034.
- [8] J. Sanz-Bermejo, J. Muñoz-Antón, J. Gonzalez-Aguilar, and M. Romero, "Optimal integration of a solid-oxide electrolyser cell into a direct steam generation solar tower plant for zero-emission hydrogen production," *Appl. Energy*, vol. 131, pp. 238–247, 2014, doi: 10.1016/j.apenergy.2014.06.028.

- [9] A. A. AlZahrani and I. Dincer, "Design and analysis of a solar tower based integrated system using high temperature electrolyzer for hydrogen production," *Int. J. Hydrogen Energy*, vol. 41, no. 19, pp. 8042–8056, 2016, doi: 10.1016/j.ijhydene.2015.12.103.
- [10] A. Mohammadi and M. Mehrpooya, "Thermodynamic and economic analyses of hydrogen production system using high temperature solid oxide electrolyzer integrated with parabolic trough collector," *J. Clean. Prod.*, vol. 212, pp. 713–726, 2019, doi: 10.1016/j.jclepro.2018.11.261.
- [11] M. Lin and S. Haussener, "Techno-economic modeling and optimization of solar-driven high-temperature electrolysis systems," *Sol. Energy*, vol. 155, pp. 1389–1402, 2017, doi: 10.1016/j.solener.2017.07.077.
- [12] J. Xu, Q. Li, H. Xie, T. Ni, and C. Ouyang, "Tech-integrated paradigm based approaches towards carbon-free hydrogen production," *Renew. Sustain. Energy Rev.*, vol. 82, no. July 2017, pp. 4279–4295, 2018, doi: 10.1016/j.rser.2017.06.029.
- [13] H. Ghezal-Ayagh, "Modular SOEC System for Efficient H₂ Production at High Current Density' 2020 DOE Hydrogen and Fuel Cells Program Review. https://www.hydrogen.energy.gov/pdfs/review20/ta019_ghezal-ayagh_2020_p.pdf."
- [14] H. Zhu and R. J. Kee, "Modeling Protonic-Ceramic Fuel Cells with Porous Composite Electrodes in a Button-Cell Configuration," vol. 164, no. 13, pp. 1400–1411, 2017, doi: 10.1149/2.0591713jes.
- [15] V. Menon, V. M. Janardhanan, and O. Deutschmann, "A mathematical model to analyze solid oxide electrolyzer cells (SOECs) for hydrogen production," *Chem. Eng. Sci.*, vol. 110, pp. 83–93, 2014, doi: 10.1016/j.ces.2013.10.025.
- [16] National Renewable Energy Laboratory, "System Advisor Model Version 2020.11.29." Golden, CO, 2020. [Online]. Available: <https://sam.nrel.gov>
- [17] W. T. Hamilton, A. M. Newman, M. J. Wagner, and R. J. Braun, "Off-design performance of molten salt-driven Rankine cycles and its impact on the optimal dispatch of concentrating solar power systems," *Energy Convers. Manag.*, vol. 220, no. July, p. 113025, 2020, doi: 10.1016/j.enconman.2020.113025.